Schmitt *et al. Heritage Science* (2022) 10:99
https://doi.org/10.1186/s40494-022-00733-2

Heritage Science

RESEARCH

Open Access

New insights into the deterioration of TiO_2 based oil paints: the effects of illumination conditions and surface interactions

Thomas Schmitt[1], Francesca Rosi[2], Edoardo Mosconi[2], Ken Shull[1], Simona Fantacci[2], Costanza Miliani[3*] and Kimberly Gray[4*]

Abstract

Titanium dioxide (TiO_2) has been used in numerous paintings since its creation in the early 1920s. However, due to this relatively recent adoption by the art world, we have limited knowledge about the nature and risk of degradation in museum environments. This study expands on the existing understanding of TiO_2 facilitated degradation of linseed oil, by examining the effect of visible light and crystallographic phase (either anatase or rutile) on the reactivity of TiO_2. The present approach is based on a combination of experimental chemical characterization with computational calculation through Density Functional Theory (DFT) modeling of the TiO_2-oil system. Attenuated Total Reflection Fourier Transform Infrared Spectroscopy (ATR-FT-IR) enabled the identification of characteristic degradation products during UV and visible light aging of both rutile and anatase based paints in comparison to $BaSO_4$ and linseed oil controls. In addition, cratering and cracking of the paint surface in TiO_2 based paints, aged under visible and UV–vis illumination, were observed through Scanning Electron Microscopy (SEM). Finally, Density Functional Theory (DFT) modeling of interactions between anatase TiO_2 and oleic acid, a fatty acid component of linseed oil, to form a charge transfer complex explains one possible mechanism for the visible light activity observed in artificial aging. Visible light excitation of this complex sensitizes TiO_2 by injecting an electron into the conduction band of TiO_2 to generate reactive oxygen species and subsequent degradation of the oil binder by various mechanisms (e.g., formation of an oleic acid cation radical and other oxidation products).

Keywords: Titanium white, Oil paint, Rutile, Anatase, Photocatalytic degradation, Visible light sensitization

*Correspondence: costanza.miliani@cnr.it; k-gray@northwestern.edu

[3] Istituto CNR di Heritage Science (CNR-ISPC), Via Cardinale Guglielmo Sanfelice 8, 80134 Naples, Italy
[4] Department of Civil and Environmental Engineering, Northwestern University, 2145 Sheridan Road, Evanston, IL 60208, USA
Full list of author information is available at the end of the article

Graphical Abstract

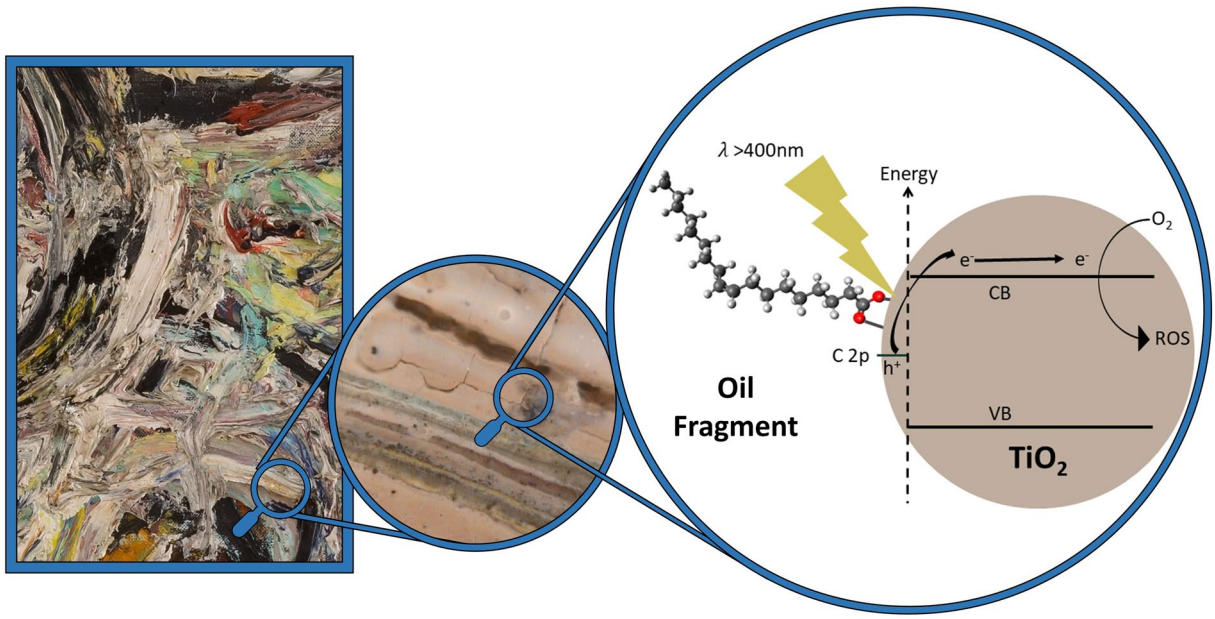

Introduction

Since the early twentieth century, titanium dioxide (TiO_2) has become the most common white pigment for both artist and commercial paints due to its high hiding power, non-toxic nature, and reasonable cost [1, 2]. TiO_2 is found in many modern works, including Piet Mondrian's *Broadway Boogie Woogie* (1942–1943) and *Victory Boogie Woogie* (1944), and many works by Jackson Pollock, including his 1947 drip masterpiece *Alchemy* [3–5]. A recent analysis of Pollock's *Eyes in the Heat* (1946), shown in Fig. 1, revealed areas containing TiO_2 which showed signs of degradation. The degradation presents as yellowing, cracking, and a chalked appearance, similar to that identified in previously published research [6–8].

TiO_2 is present in paintings primarily as one of two crystalline structures: anatase or rutile. Both phases were found in *Eyes in the Heat* by in-situ measurements through a portable Raman system and shown in the insert of Fig. 1. Anatase was first produced in 1914 and is the more photo-reactive phase. Over time, the production of TiO_2 based white paints switched to the less photocatalytically active rutile phase [1]. In addition to being a pigment, TiO_2 is a semiconductor and facilitates the formation of radical oxygen species (ROS) under ultra-band gap illumination [9]. For anatase, the ultra-band gap illumination is limited to near UV light ($\lambda < 385$ nm), whereas rutile has a tail that extends the response into visible light ($\lambda < 410$ nm) [9]. While it is widely reported that anatase has lower rates of recombination and hence, higher photo-reactivity than rutile, these differences may be diminished under certain conditions and both materials may generate radical products that promote degradation of the oil binder [10–14]. Furthermore, the behavior of semiconductor pigments such as TiO_2 is influenced by interactions with other components present in the complex matrix of a paint film, such as inorganic and organic compounds. These interactions can result in charge transfer complexes such as those studied in solar cell applications and are well documented to extend the response of TiO_2 into visible light [15–19].

In order to probe the pathway of paint deterioration under various illumination conditions, we studied the complex TiO_2-binder interactions under visible and UV light with a combined experimental and computational approach. We monitored chemical and morphological changes using FT-IR spectroscopy and electron microscopy to investigate the effects of aging anatase and rutile pigments in linseed oil based model systems under three lighting conditions: UV and visible light (UV–vis, $\lambda > 350$ nm), visible light (vis, $\lambda > 400$ nm) and dark. Control experiments with both pure linseed oil and $BaSO_4$ based paints were also conducted. The experimental approach was complemented by Density Functional Theory (DFT) based calculations. The calculations were

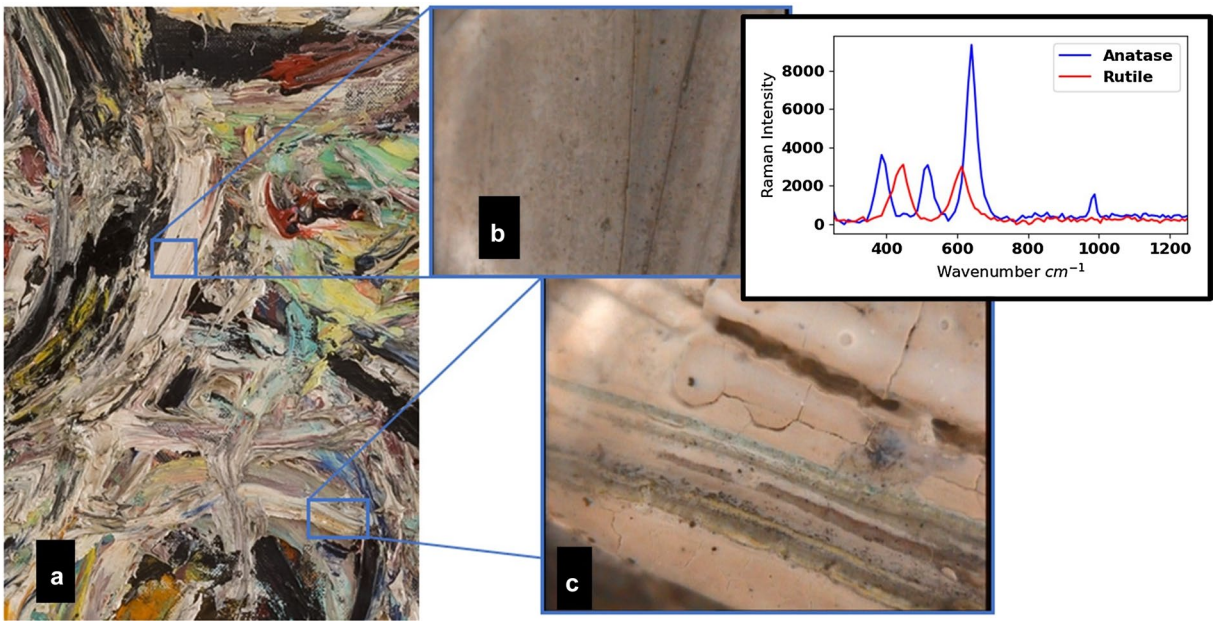

Fig. 1 **a** Section of *Eyes in the Heat* (1946) painted by Jackson Pollock. Inserts show an area of **b** rutile based paint and **c** an area of anatase based paint, inset shows the Raman spectra used to confirm the polymorph in each area

performed on anatase TiO_2 and oil components individually, and on oil adsorbed to the TiO_2 surface to probe the photochemical effects of surface interactions between oil and TiO_2.

Materials and methods

Aging experiments

Model paint-outs were created by mixing the selected pigment with linseed oil (Sigma-Aldrich CAS 8001-26-1) using a palette knife on a glass plate. Pigments were mixed at pigment weight concentrations of 25% for rutile TiO_2 (Strem Chemicals CAS 13463-67-7, > 100 nm primary particle size, 99% purity) and anatase TiO_2 (J.T. Baker Material No. 4162-01, < 25 nm primary particle size, 99.7% purity) and 30% for $BaSO_4$ (Sigma-Aldrich CAS 7727-43-7, 99.1% purity). To simplify the system while remaining relevant to *Eyes in the Heat*, coated TiO_2 pigments and commercially available titanium white were not studied. The paint mixture was blade coated onto 2 cm × 2 cm Lexan polycarbonate squares at a nominal thickness of 250 µm. The coated paint-outs were left to cure for 1 month in the ambient lab environment (~ 50% RH and 22 °C). Following the methods outlined in de Viguerie et al. [20], polymerization was confirmed after 1 month by monitoring the absence of the =C–H cis stretch peak at 3010 cm^{-1} with Fourier Transform Infrared Spectroscopy in Attenuated Total Reflection mode (ATR-FT-IR).

Samples were aged for a total of 2 months in a custom designed illumination apparatus constructed of polycarbonate chambers, shown in Additional file 1: Fig. S1. The chambers were controlled and monitored to be at 25 ± 1 °C and 50 ± 5% RH. Lighting conditions were fixed through a single mounted 400 W metal halide lamp (Slyvania M400/U), with either a Pyrex filter to remove wavelengths below 350 nm for UV–vis light, or a UV blocking filter (Edmund optics UV filter sheet) to remove wavelengths below 400 nm for visible light aging. The intensities of the UV ($350 < \lambda < 400$ nm) and visible ($\lambda > 400$ nm) portions of the spectra were 232 µW cm^{-2}, and 6.33×10^4 µW cm^{-2}, respectively. The spectra for the UV–vis and visible lighting conditions are illustrated in the Additional file 1: Figs. S2 and S3. One chamber was covered with blackout optics cloth to achieve dark conditions.

All samples were characterized every ~ 8 days through micro ATR-FT-IR using a Bruker LUMOS II equipped with a 100 µm germanium crystal. Spectra consisted of an average of 32 scans from 4000 to 600 cm^{-1} with a resolution of 4.0 cm^{-1} and low ATR pressure. Surface spectra were obtained from 6 positions across the sample and once the spectral reproducibility was verified, they were averaged. Spectra were then baseline corrected and normalized to the 1736 cm^{-1} carbonyl peak.

SEM images were taken with field emission scanning electron microscope LEO 1525 by ZEISS, GEMINI column. Before imaging with the SEM, samples were

coated with 5 nm of carbon to prevent charging due to the low electrical conductivity of linseed oil.

Computational details and models

Anatase TiO_2, the fatty acids composing linseed oil shown in Additional file 1: Fig. S4 (oleic, linoleic, and linolenic acids), and oleic acid attached to the TiO_2 surface were modeled computationally. Each component's structure, including bond angles, atomic spacing, and cell dimensions, was optimized and the subsequent electronic properties were analyzed.

The TiO_2 model was optimized using Quantum Espresso [21] within the generalized gradient approximation (GGA) and the Perdew-Burke-Ernzerhof (PBE) [22] exchange correlation (xc) functional, as reported in Vittadini et al. [23] Electron–ion interactions were modeled using Vanderbilt ultrasoft pseudopotentials [24]. The plane wave basis set cutoff energy was set to 25.0 Ry and the charge density and potential kinetic energy cutoff was set to 200 Ry. Davidson iterative diagonalization with overlap matrix was used with a convergence threshold of 1.0×10^{-6} and a 0.2 mixing factor. Initial calculations were done on a $(TiO_2)_{64}$ slab of 2 TiO_2 (101) layers each with 4 rows of five- and six- coordinated Ti sites. The (101) surface was chosen as it is naturally the majority exposed surface in anatase [23]. Periodic boundary conditions were applied in the x, y, and z dimensions. To simulate an exposed top surface, the z cell dimension was increased by 10 Å. Only the Γ-point was considered for all calculations. Convergence calculations for z cell dimension and k point sampling are included in the Additional file 1: Fig. S5.

The oleic, linoleic, and linolenic acids were optimized using Gaussian 09 (G09) [25], the B3LYP [26–29] exchange correlation functional, and the 6–31(d,p) [30] basis set. Calculations on the oleic acid was repeated using the PBE functional [20] and the 6–31(d,p) [30] basis set to compare with the TiO_2 periodic calculation. The electronic structure of the three acids was analyzed in terms of energy and character of the frontier molecular orbitals, to evaluate the possibility of charge transfer between the acid and the TiO_2 (101) slab. Avogadro software was employed to plot the molecular orbitals by using an iso-density surface cutoff of 0.02 [31].

Density of States (DOS) and partial Density of States (pDOS) calculations were performed using Quantum Espresso's DOS.x postprocessing program. A Gaussian broadening of 0.02 Ry and an energy grid step of 0.1 eV were used.

Results

Aging results

For all samples and aging conditions, explicit attention was paid to the characteristic markers of oxidation products in FT-IR spectra: the formation of a spectral feature at 1710 cm^{-1} assigned to C=O stretching of carboxylic acids and aldehydes, the formation of a broad shoulder centered around 1776 cm^{-1} attributed to the C=O stretching of peracids, peresters, γ-lactones, and anhydrides, the formation of a broad shoulder between 1670 and 1610 cm^{-1} assigned to ν(C=C) of conjugated dienes, and changes to peaks in the region around 1168 cm^{-1} associated with triglyceride ester linkages [6, 32, 33]. These spectral markers were associated with the degradation of linseed oil through β-scission reactions and γ-lactones formation reactions proposed by Van Driel [3]. The broad region between 1670 and 1610 cm^{-1} contains multiple peaks including ν(C=C) of conjugated diene compounds which has been previously attributed to the degradation of linseed oil [32, 34–40]. For the purposes of comparing peak intensity, the region 1670–1610 cm^{-1} is measured at 1640 cm^{-1}.

For the linseed oil only samples (Fig. 2a and b) and the samples made with non-photoreactive $BaSO_4$ (Additional file 1: Fig. S6), the FT-IR spectra show changes consistent with hydrolysis and direct photolysis as reported in previous research [41]. Hydrolysis and direct photolysis generate free fatty acids through auto-oxidation and β-scission reactions which can be observed as slight shoulders forming at 1710 cm^{-1} and 1776 cm^{-1} in Fig. 2a and b. In the oil paint samples, very small changes were observed in the 1168 cm^{-1} peak associated with triglyceride ester linkages. Under visible illumination (Fig. 2a) the 1168 cm^{-1} peak is stable until the last exposure point where the intensity decreases slightly. Under UV–vis illumination (Fig. 2b) the 1168 cm^{-1} peak increases slightly for the first three exposure amounts and then decreases for the last exposure. In the $BaSO_4$ pigmented samples shown in Additional file 1: Fig. S6, the triglyceride ester linkage peaks are obscured by the contribution of the sulfate peaks and therefore no conclusions can be made about the changes of the triglyceride ester linkages with aging in these samples. The linseed oil sample illuminated with visible light (Fig. 2a) shows the slight formation of a broad shoulder between 1670 and 1610 cm^{-1}. Interpretation of this region's degradation products is not trivial because of overlapping spectral features. Hayati et al. has attributed some features in this region to reaction products of the polyunsaturated fatty acid components of linseed oil such as the ν(C=C) of conjugated diene compounds formed by processes similar to autooxidation [42]. Meilunas et al. attributed this more specifically to β-unsaturated carbonyl compounds [32]. Both compounds could form through allylic hydrogen abstraction as mediated by OH radicals and subsequent oxygen mediated conversion from an unconjugated to conjugated structure [40, 42, 43]. However, the UV–vis

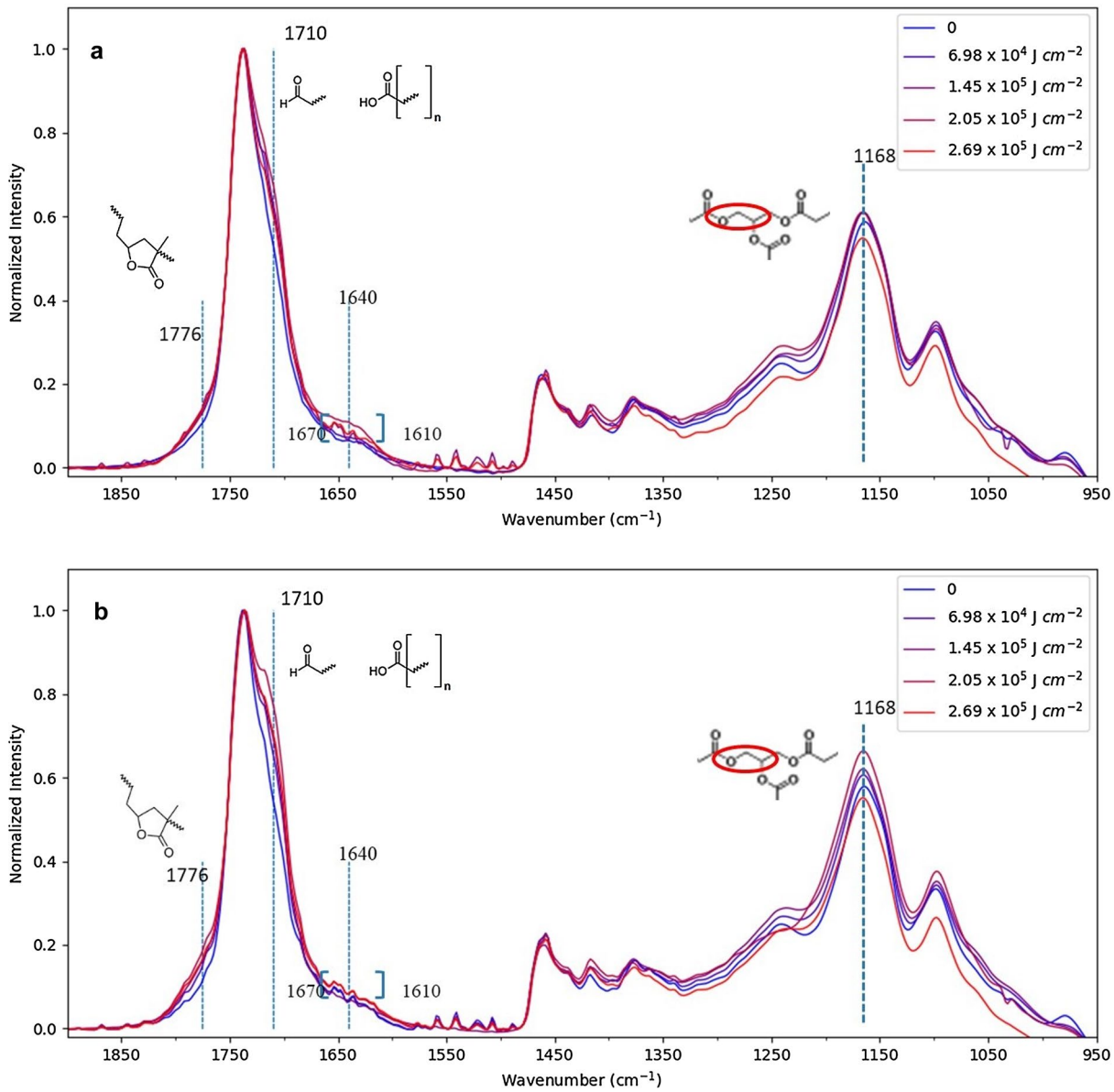

Fig. 2 Linseed oil aged in **a** vis, and **b** UV–vis conditions. Characteristic markers of degradation are marked with dotted lines and functional groups showed minimal changes over the same aging period as seen in the Additional file 1: Fig. S8

illuminated linseed oil sample (Fig. 2b), and both UV–vis and visible illuminated $BaSO_4$ samples (Additional file 1: Fig. S6) show no appreciable changes in this region. This suggests, as expected, that the conversion of unconjugated to conjugated carbon bonds is not significant in the control samples of pure linseed oil and $BaSO_4$.

A number of interesting results were observed when comparing linseed oil with TiO_2 containing samples (Fig. 3). First, evidence of degradation was seen both in samples exposed to visible light (Fig. 3a) and samples exposed to UV–vis conditions (Fig. 3b) after 269 kJ cm^{-2} of aging. Second, the telltale signs of degradation were observed for both anatase and rutile based paints. As shown in Additional file 1: Fig. S7, under visible and UV–vis illumination both rutile and anatase based paints showed the formation of a shoulder at 1710 cm^{-1} which evolved to a strong peak with increasing exposure, suggesting that both anatase and rutile promote the formation of free fatty acids. The degradation of the TiO_2 pigmented oil is also evident in Additional file 1: Fig. S7 by observing the growth of peaks in the 1670–1610 cm^{-1} region due to autooxidation

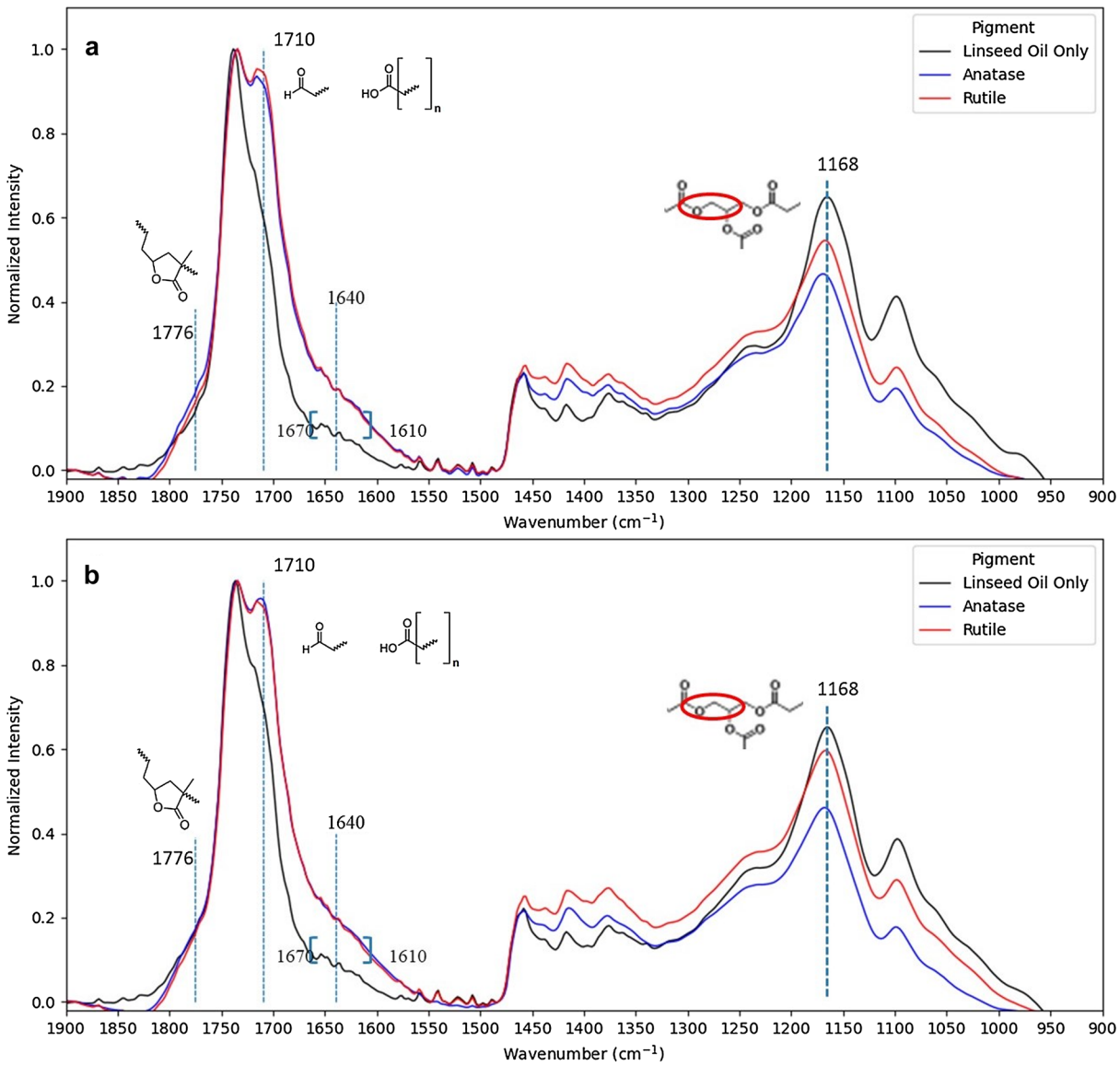

Fig. 3 Linseed oil only, anatase, and rutile based paint aged in **a** visible and **b** UV–vis light with a total exposure of 269 kJ cm^{-2}. Characteristic markers of degradation are marked with dotted lines and functional groups

as described above. The growth of peaks in this region observed in both Fig. 3a and b and Additional file 1: Fig. S7 suggests that anatase and rutile based paints promote the degradation of oil through the acceleration of OH radical generation under both visible and UV–vis light conditions driving the conversion of unconjugated carbon bonds to conjugated bonds in polyunsaturated fatty acids. The linseed oil only sample (Fig. 2a and b) shows little to no growth in this region. Also, as opposed to pure linseed oil (Fig. 2), anatase and rutile based samples (Fig. 3) showed a marked decrease in the main peak at 1168 cm^{-1} for both UV–vis and visible light exposed samples indicating a degradation of the triglyceride ester linkage bond as a function of exposure. Dark aged samples.

The rate of degradation can be evaluated by plotting the intensity of the 1710 cm^{-1} peak and 1670–1610 cm^{-1} region (as measured at 1640 cm^{-1}). These plots, shown in Fig. 4a and b, clearly demonstrate that both rutile and anatase TiO_2 based pigments facilitate oil degradation in both the visible and UV–vis light conditions.

There are two noteworthy differences between the spectral trends for linseed oil only samples and those with TiO_2 in Fig. 4. First, TiO_2 based paints demonstrated

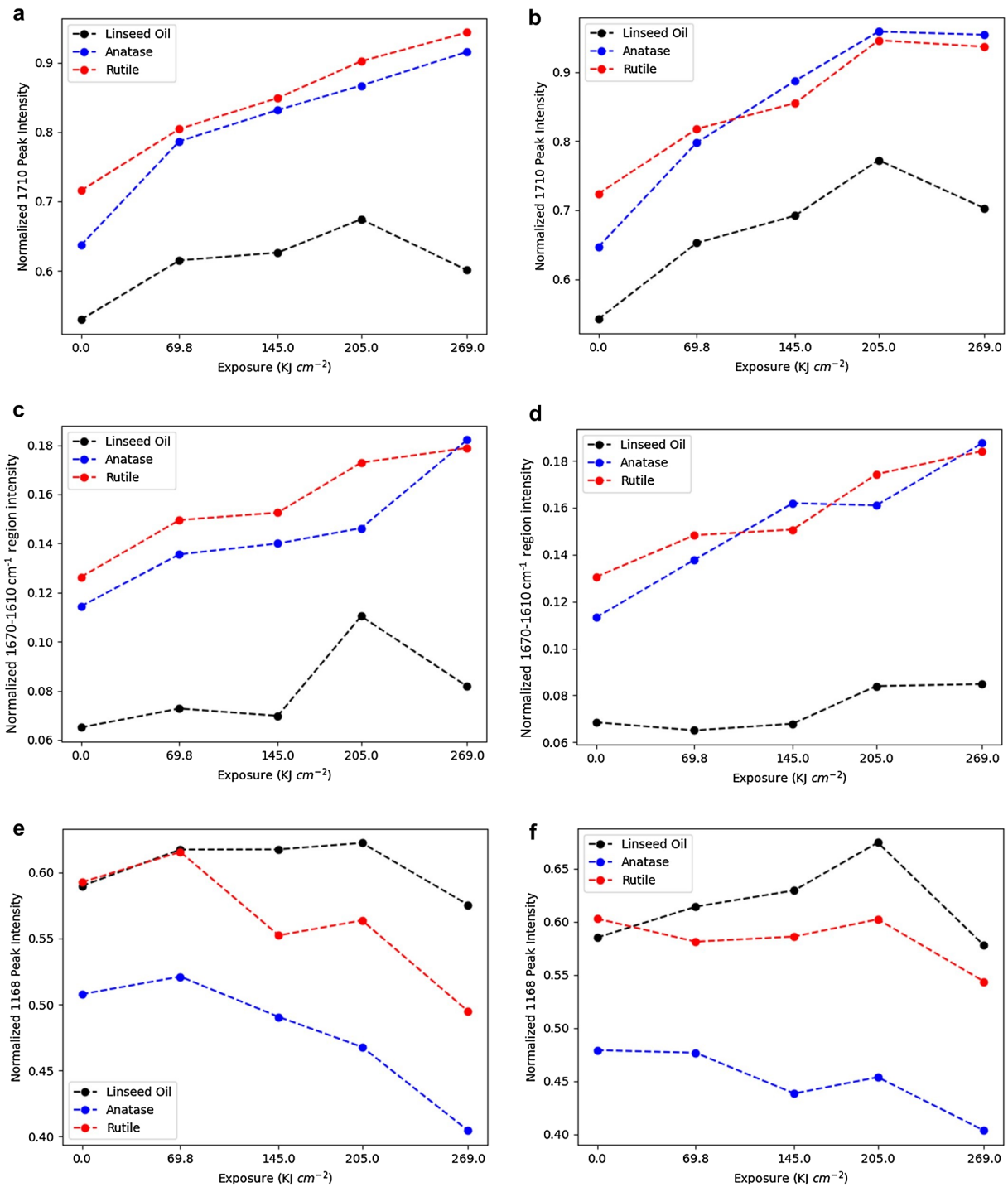

Fig. 4 Change in the intensity for the 1710 cm^{-1} peak, the 1670–1610 cm^{-1} region measured at 1640 cm^{-1}, and the 1168 cm^{-1} peak in **a**, **c**, **e** visible light and in **b**, **d**, **f** UV–vis light. The considered bands are normalized to the 1736 cm^{-1} ester peak

a higher initial peak intensity for both spectral features compared to linseed oil. This may indicate adsorption of fatty acids to the TiO_2 surface prior to light exposure. Second, the rate of degradation, as measured by the change in the 1710 cm^{-1} free fatty acid peak intensity, is higher for TiO_2 pigmented samples than pure linseed oil for both light aging conditions (Fig. 4a and b). Additionally, the peaks formed more rapidly in UV–vis exposed

samples shown in Fig. 4b, resulting in a steeper slope when fitted with a linear regression than Fig. 4a. Linseed oil had approximately double the slope under UV–vis light (Fig. 4b) compared to visible (Fig. 4a). Anatase's slope showed an increase of about 1.2 times from visible exposure to UV–vis exposure. Interestingly, rutile shows nearly identical slopes under visible exposure and UV–vis exposure according to the linear regression, indicating that the UV component of the light does not have a strong effect on the formation of these free fatty acids by rutile.

The spectral region from 1670 to 1610 cm^{-1} as seen in Fig. 4c and d exhibits similar trends. Both anatase and rutile based paints show strong increases in intensity for this region as a function of exposure of both visible (Fig. 4c) and UV–vis light (Fig. 4d) similar to the 1710 cm^{-1} peak. As a contrast to the 1710 cm^{-1} peak, the slope of the 1640 cm^{-1} peak height versus exposure for both UV–vis exposed TiO_2 based paints is approximately double that of the visibly exposed samples indicating that UV–vis light plays a larger role in the generation of the degradation products attributed to this region.

Linseed oil only samples show a moderate increase followed by a decrease in this 1670–1610 cm^{-1} region for visibly aged samples (Fig. 4c) and a slight increase for UV–vis aged samples (Fig. 4d). Small sinusoidal noise in the FT-IR spectra for the 205 kJ cm^{-2} and 269 kJ cm^{-2} exposed linseed oil samples made the peak heights difficult to measure resulting in a more variable linear regression between samples. As a result, we are treating the trend as linear. $BaSO_4$ based samples, showed no increase in intensity for the 1670–1610 cm^{-1} region and slight increase in 1710 cm^{-1} peak height in UV–vis illuminated samples as can be seen in the Additional file 1: Fig. S6. We have observed free fatty acid formation as evidenced by the slight increase in 1710 cm^{-1} peak intensity for linseed oil in Fig. 4b, and the increase in the same peak for UV–vis illuminated $BaSO_4$ samples in Additional file 1: Fig. S6. This suggests that direct photolysis of linseed oil also facilitates the formation of free fatty acids. However, the more than two-fold difference in rate of formation of the free fatty acids and the formation of conjugated dienes distinguishes TiO_2 facilitated degradation from direct photolysis of linseed oil.

The region corresponding to the triglyceride ester linkages (1300–1000 cm^{-1}) shows different behavior for each condition as seen in Fig. 4. Interpreting the peaks in this region is difficult because this region contains peaks corresponding to multiple structures and competing processes; however, some clear trends appear. Both anatase and rutile TiO_2 pigmented samples show a decrease in the intensity of the 1168 cm^{-1} peak over exposure to both visible (Fig. 4e) and UV–vis light (Fig. 4f). Interestingly, the change in peak intensity is greater for both TiO_2 polymorphs samples illuminated with visible light. The rate of diminishment of this band is similar for anatase and rutile based paints, indicating that, especially under visible illumination where the slope is greatest, the primary driver of degradation is not the inherent activity of the TiO_2 polymorph, but instead some other mechanism such as the formation of a charge transfer complex as will be discussed in Section "Computational results". Pure linseed oil shows no significant change in visible light as shown in Fig. 4e. Under UV–vis illumination pure linseed oil shows slight peak growth then rapid decline. These data show that the scission of this linkage is unique to TiO_2 facilitated degradation.

Under all conditions, when observed optically, the surface of the aged paint was relatively smooth with no visible cracks, craters, or particles. However, when observed under SEM, both anatase and rutile TiO_2 oil samples, aged under both UV–vis and visible light, show signs of degradation. A significant oil loss is visible as small clusters of pigment (Fig. 5a) in the UV–vis light aged anatase samples characterized also by large cracks and voids in agreement with previously reported results [8]. Notably we also observed in rutile based samples (Fig. 5b), larger pigment particle clusters and small voids when exposed to UV–vis light. This is consistent with the FT-IR results which show that rutile based paint shows degradation similar to anatase. SEM images also demonstrate that also visible light influences the surface of the paint independently from the TiO_2 polymorph showing for both anatase and rutile oil paints early signs of oil loss in visibly illuminated samples. Due to the lack of particles, linseed oil films were difficult to observe under electron microscopy. Instead, paints pigmented with the photocatalytically inert $BaSO_4$ (Fig. 5c) show unchanged surfaces with few signs of degradation and no clear effects due to differing lighting conditions indicating that direct photolysis of linseed oil does not account for the oil degradation and loss seen in TiO_2 pigmented samples.

Computational results

Although photocatalytic reactions are expected under the UV irradiation of anatase pigments, it was surprising to observe pigment deterioration under visible light [3, 6]. To explain this observation, we used DFT methods to model the structural and electronic properties of linseed oil and anatase TiO_2 as well as the interactions between them to investigate possible photochemical pathways to linseed oil degradation under visible light.

Using Quantum Espresso [21] the anatase slab geometry was optimized using computational details described in Section "Computational details and models". The energy levels were calculated, resulting in a band gap of

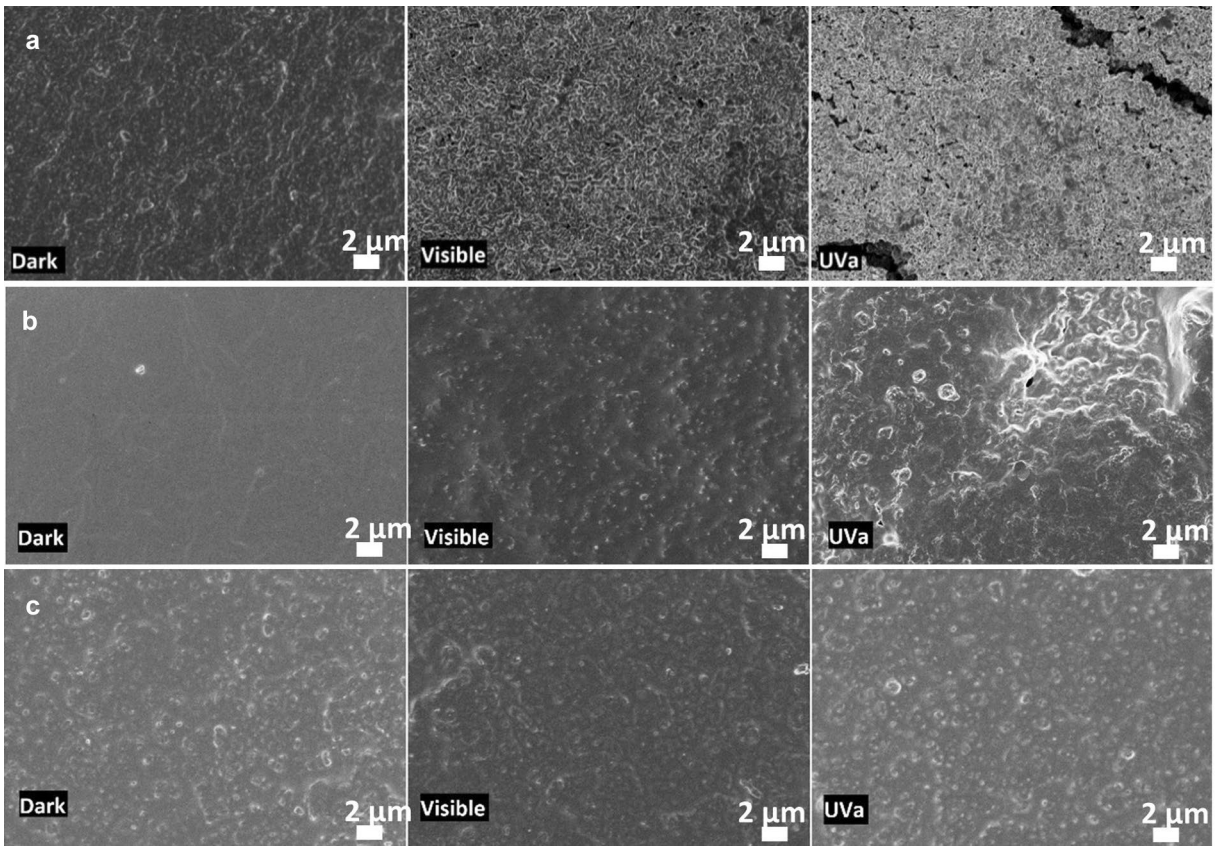

Fig. 5 SEM images at 36 days aged in various lighting conditions (Visible light—197 kJ cm^{-2}, UV light—721 J cm^{-2}) for **a** anatase, **b** rutile, and **c** $BaSO_4$ oil paints

1.91 eV. This is underestimated with respect to the experimental value for anatase TiO_2 (3.2 eV), but in line with band gaps computed using GGA exchange–correlation functions. [9, 44]

The structural and electronic properties of oleic, linoleic, and linolenic acids were calculated using the Gaussian 09 package as described in Section "Computational details and models". In Fig. 6a, we report the energies and isodensity plots of the highest occupied molecular orbitals (HOMO) and HOMO − 1, and of the lowest unoccupied molecular orbitals (LUMO) and LUMO + 1 for oleic, linoleic, and linolenic acids computed with the B3LYP exchange–correlation functional. For all oil fragments, the HOMO is delocalized on the unsaturated bond. For oleic acid, the LUMO is delocalized on the carboxyl group, while for linoleic and linolenic the LUMO is delocalized on the unsaturated bonds. For linoleic and linolenic acids, the LUMO + 1 is delocalized around the carboxylic acid group. However, the LUMO energy of the oleic acid is almost isoenergetic with respect to the LUMO + 1 energy of linoleic and linolenic acid. In this case, it is more useful to compare the LUMO of oleic acid with the LUMO + 1 of the other two component acids.

The energy levels of the HOMOs for the three linseed oil components are within ~ 1 eV of each other. The energy levels of the HOMOs and LUMOs for calculations of both B3LYP and PBE functionals for oleic acid are summarized in Table 1. The energy levels for the other component acids as calculated with B3LYP functional are presented in the Additional file 1: Table S1. The PBE functional underestimates the HOMO–LUMO energy gap for oleic acid as expected. However, both PBE and B3LYP HOMO–LUMO gap for all the fatty acids correspond to deep UV light.

Oleic acid was chosen to model the interaction between TiO_2 and the linseed oil as it is a likely free fatty acid product of the auto-oxidative curing process and because it is monounsaturated [45–47]. In the oleic acid-TiO_2 complex, the optimized oleic acid was adsorbed to the (101) surface of the TiO_2 slab in either a bidentate bridging mode or monodentate mode as shown in Fig. 6b. For the bidentate mode, the carboxylic

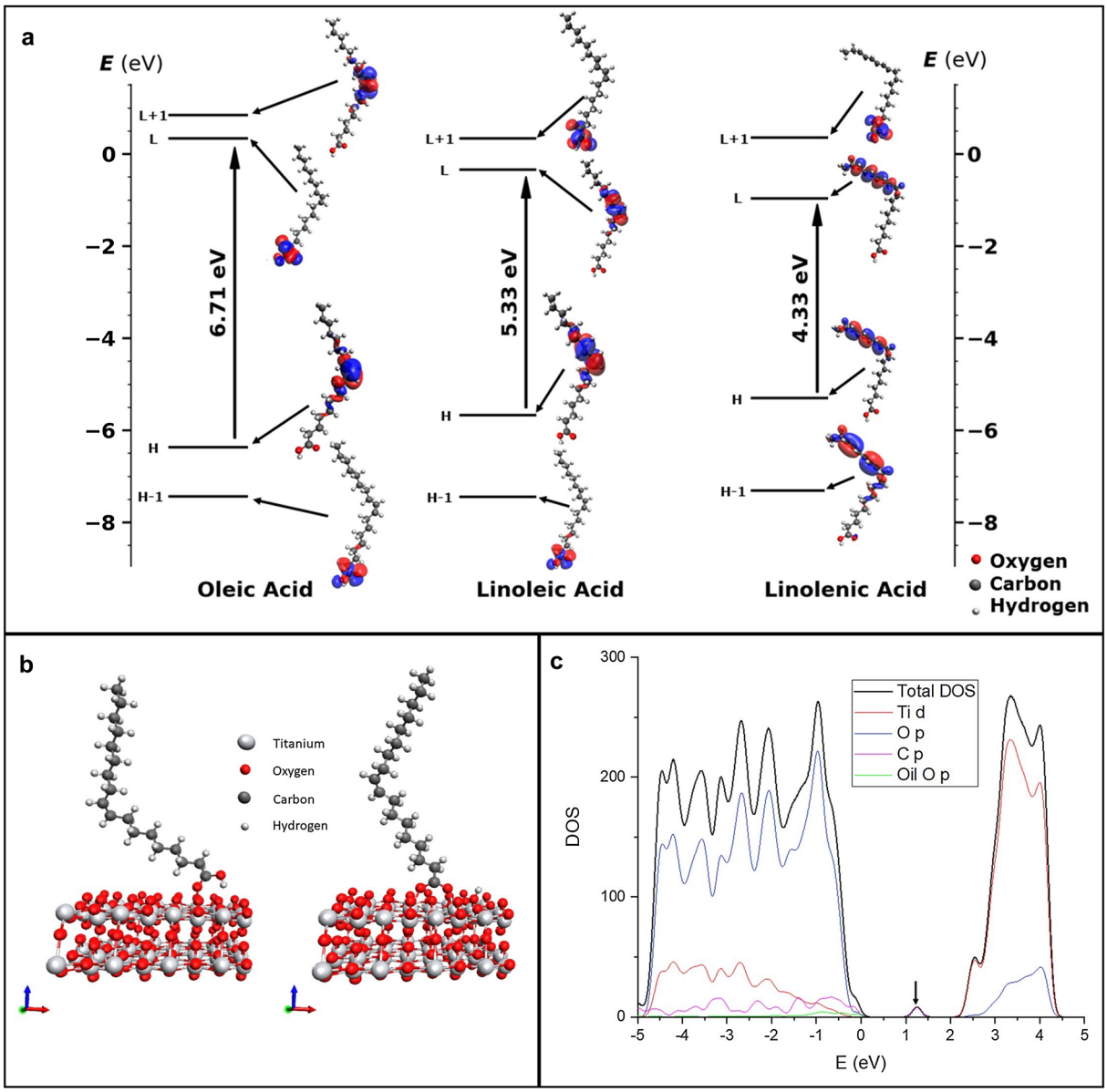

Fig. 6 **a** Main frontier orbitals energies and isodensity plots for the component acids of linseed oil. Positive spin polarization of the frontier orbitals is represented as blue and negative spin polarization is represented as red. **b** Binding modes and optimized geometry for oleic acid on the (101) surface of anatase TiO_2; monodentate (right) and bidentate (left). **c** Density of states of the oleic acid-TiO_2 complex, and the partial density of states separated contributions showing the orbital origin of the intra-band state are reported. The intra-band state is denoted by an arrow

Table 1 Frontier energy levels and HOMO–LUMO gap for linseed oil component acids calculated with B3YLP and PBE functionals

Molecule	Functional	HOMO (eV)	LUMO (eV)	$\Delta E_{H\text{-}L}$
Oleic acid	B3LYP	− 6.37	0.34	6.71
	PBE	− 5.45	− 0.64	4.81

proton was dissociated and transferred to the surface of the TiO_2 slab. It was found that the bidentate mode was more energetically favored with respect to the monodentate mode by 3.76 kcal mol^{-1}. This form was expected based on other binding modes for carboxylic acids [48, 49]. Therefore, hereafter we discuss only the oleic acid attached to the TiO_2 in bidentate configuration.

The density of states (DOS) of the oleic acid-TiO_2 system shows the presence of an intra-band occupied state located ~1.25 eV above the TiO_2 valence band. Analysis of the partial DOS (pDOS) shown in Fig. 6c reveals that this state originated from the p orbitals of the carbons in the oleic acid, allowing direct injection from the C 2p orbitals of the oleic acid into the conduction band of the TiO_2. This transition may have an excitation energy lower than anatase or oleic acid alone and low enough that excitation is possible under visible light.

Discussion

Previous results have shown that UV light degrades both linseed oil alone, and paint films containing anatase TiO_2. [41, 46, 50, 51] This research refines the understanding of photocatalytic degradation of paint pigments presented in previous literature in a number of ways. First, we have demonstrated that anatase based paint films degrade not only under UV–vis illumination, but also under the visible light conditions employed in this study. Second, although the activity of anatase based paint under UV illumination has been well documented, the more common and more modern rutile pigment is believed to be photocatalytically inactive [8, 13]. We have presented evidence of the photocatalytic activity of rutile based paint films in both visible and UV light under our experimental conditions that revises this thinking. Third, by investigating computationally the complex interactions between the pigment and binder we simulate a possible mechanism of the visible light activity observed experimentally in anatase based paints and suggest that a similar mechanism may explain the visible light activity seen in rutile based paints. Fourth, the lighting conditions used in this study have a much lower intensity than the conditions used in previous studies [6, 8, 12, 52]. These milder lighting conditions allowed us to probe, in greater detail, the degradation of linseed oil in the presence of TiO_2 by diminishing the contribution of direct photolysis allowing the effect of TiO_2 to dominate, and by slowing the rates of reactions to allow us to follow initial photochemical transformations. As a result, we have gained greater insight into the kinds of reactions that may unfold over prolonged exposure to low intensity interior lighting.

Our experiments explicitly probed photochemical reactions under visible light, whereas this has not been considered previously in the context of TiO_2 paint photocatalysis. The activity we observed for TiO_2 (both anatase and rutile) based paints under visible light is noteworthy for several reasons. The ΔE_{BG} for anatase is 3.2 eV, which corresponds to UV light of wavelengths less than 385 nm. [9] The mechanism of TiO_2 facilitated paint degradation published by Van Driel et al. and others suggest that anatase would not be active in visible light due to a lack of ultra-band gap illumination [53–56]. The same proposed mechanism suggests that although rutile may absorb visible light below 410 nm, rutile's photocatalytic activity is less than anatase's due to a lower degree of band bending at the surface resulting in higher rate of charge recombination [57]. However, the experimental evidence presented in this study indicates that the two components that are individually inactive in visible light become active when combined with linseed oil suggesting that other mechanisms are at play.

We propose the formation of a charge transfer complex, as presented computationally in this study, leading to an occupied orbital within the TiO_2 band gap and effectively lowering the required ultra-band gap energy and allowing visible light ($\lambda > 400$ nm) to excite an electron into the conduction band of the TiO_2. Because the contribution of this intra-band state derives from the occupied C 2p orbital, it can be inferred that a similar state will be created with anatase TiO_2 and linoleic and linolenic acids due to the similar energetic levels of the C 2p orbital in these fragments.

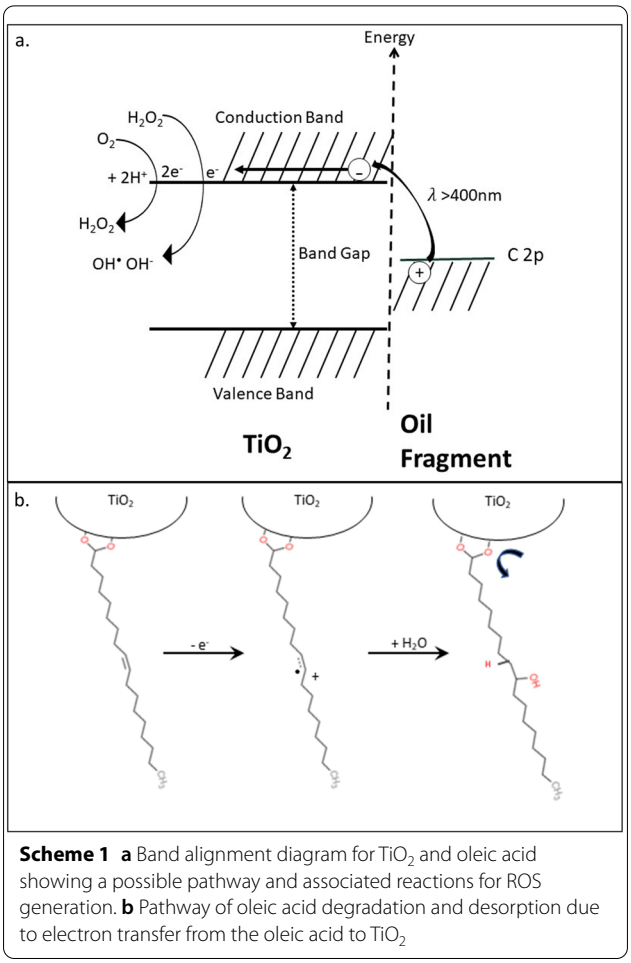

Scheme 1 **a** Band alignment diagram for TiO_2 and oleic acid showing a possible pathway and associated reactions for ROS generation. **b** Pathway of oleic acid degradation and desorption due to electron transfer from the oleic acid to TiO_2

Table 2 Assignment of the main spectral changes observed in linseed oil aging and summary of the observed changes

Functional group	Peak position (cm^{-1})	Assignment	Observed changes in linseed oil and $BaSO_4$	Observed changes in TiO_2
C=O stretch	1776	Peracids, perester, γ-lactones, and anhydrides	Small increase in visible and UV–vis light	Small increase in visible and UV–vis light
	1736	Ester	Used for normalization	Used for normalization
	1710	saturated ketones, COOH acid, and aldehydes	Minimal increase in linseed oil and $BaSO_4$ samples in UV–vis and visible light; No changes in dark	Large increase in UV–vis and visible light; Slight increase in dark, final point for anatase UV–vis shows large increase
C=C	1670–1610	ν (C=C) of β-unsaturated carbonyl compounds	Small increase in linseed oil only samples in visible and UV–vis light	Strong increase in anatase and rutile pigmented samples in visible and UV–vis light; minimal increase in dark
ν (C–O) Triglyceride ester linkage	1000–1300 (main peak at 1168)	ν(C–O) in triglyceride ester linkage + ν_{as} (C–O) of C–C(O)–O	Slight increase followed by decrease in linseed oil only samples, N/A in $BaSO_4$ samples	Decrease in TiO_2 containing samples in UV–vis and visible light.; No clear change in dark

This charge transfer complex between anatase and oleic acid allows for the formation of reactive oxygen species (ROS) needed for the characteristic β-scission reactions, as illustrated in Scheme 1a. It is important to note that the lack of a hole in the TiO_2 valence band prevents the formation of hydroxide radicals due to the oxidation of water, since there is no electron vacancy in the TiO_2. Rather, a proton assisted two electron transfer to oxygen from the TiO_2 conduction band forms hydrogen peroxide, and through sequential charge transfer reactions such as presented in Scheme 1a and below, hydroxide radicals can be formed via an alternative route.

$$O_2 + e^- + H^+ \rightarrow HO_2^{-\cdot}$$

$$HO_2^{-\cdot} + e^- + H^+ \rightarrow H_2O_2$$

$$H_2O_2 + e^- \rightarrow OH^{\cdot} + OH^-$$

The charge vacancy in the C 2p orbital of the oleic acid resulting from the electron transfer into the TiO_2 can lead to yet another mechanism for degradation. After charge injection, the oleic acid forms a cation radical with an unpaired electron located on the previously unsaturated carbon. As shown in Scheme 1b, a reaction with water results in hydroxylation of the oleic acid radical and desorption from the TiO_2 surface in Scheme 1b. It may also lead to oxidative degradation similar to that outlined by Dlugogorski et al. [58].

In addition to the visible light activity of TiO_2 based paints, it was also interesting that rutile, one of the most common white pigments today, exhibited rates of degradation similar to anatase [59]. The lower photo-reactivity of rutile is attributed to higher charge recombination rates relative to anatase [12]. This has led many conservators and scientists to dismiss rutile based paints as degradation risks [6, 8, 34, 52]. However, an interaction between rutile and oil fragments, similar to the one shown in Scheme 1a, may sensitize it to visible light by forming a charge transfer complex resulting in similar photocatalytic activity as anatase. Although the interaction of rutile and oil fragments was not investigated computationally in this study, previous results on the interaction of rutile and other carboxylic acids have shown the formation of complexes similar to those demonstrated with anatase in this study [60]. The similarity observed between rutile and anatase's visible and UV–vis light activity suggests that the sensitization of the TiO_2 may be a dominant factor for both polymorphs.

The difference in illumination conditions between the experiments of this study and previous studies provides another explanation for the photoactivity observed in the rutile based paint. Research has shown that high light intensity accelerates charge recombination [61]. Using a light (232 μW cm^{-2}) only 3% as intense as the UVA illumination employed by Morsch et al. (8 mW cm^{-2}), we achieved lower recombination rates and slower rates of reaction for both rutile and anatase based paint [6, 62]. These lower recombination rates provide another possible explanation for the increased photocatalytic activity of the rutile pigment compared to previous studies. The lower light intensities, and slower rates of reaction in comparison to other reported work allowed us to observe initial reaction phenomena that was not evident under much stronger radiation conditions. This study implemented a total UV exposure of 0.986×10^3 J cm^{-2}

over 49 days, significantly lower than the total exposure (7.3×10^3 J cm^{-2}) and even less than the first exposure (2.1×10^3 J cm^{-2}) in the work by Morsch et al. The low amount of total UV exposure used in this study suggests that the chemical and physical changes presented reflect early degradation phenomena that could not be observed in studies using much greater illumination flux. The lower intensity light also resulted in less direct photolysis of linseed oil. This allowed the distinction to be made between TiO_2 facilitated degradation of linseed oil and direct photolysis.

Previous studies have discussed that it is difficult to distinguish between hydrolysis and photocatalytic degradation through FT-IR methods alone [6]. However, the presence of unique spectral changes in TiO_2 containing samples reveals a spectroscopic differentiation between hydrolysis and photocatalytic degradation. The FT-IR differences between photo-oxidized linseed oil and TiO_2 facilitated degradation of linseed oil are summarized in Table 2. The clearest difference between TiO_2 facilitated degradation and direct photolysis of linseed oil is evident by examining the peak associated with the triglyceride ester linkage. The decrease in peak intensity indicates that, unlike direct photolysis, TiO_2 facilitated degradation breaks the C–C(O)–O ester linkage. This is a unique spectral feature that allows for the detection of TiO_2 facilitated degradation through FT-IR methods.

Anatase TiO_2 facilitated degradation is often characterized by a "chalked" surface [63, 64]. Previous studies have attributed this description to an increase in surface roughness associated with loss of oil and surfacing of pigment particles [6–8]. The SEM micrographs in this study provide more information to confirm the phenomena of oil loss and pitting. Additionally, the SEM micrographs show surface degradation of rutile based pigments, confirming its activity in both visible and UV–vis light. The presence of large cracks in the micrographs of anatase based paint suggests that microcracking of the paint may occur before large scale degradation is visible. Finally, the SEM micrographs were taken from samples with total UV–vis exposure of 7.50×10^2 J cm^{-2}. This is about 75% of the light exposure (750 J cm^{-2} vs 1050 J cm^{-2}) than has been previously studied for TiO_2 activity, indicating that damage from TiO_2 facilitated degradation occurs earlier than others have shown [8].

For these reasons, both anatase and rutile TiO_2 based pigments should be considered active in low UV and visible light environments due to surface interactions with fatty acid oil fragments. These results show that degradation of the paint film and loss of binding media may be occurring at early stages before chalking is visible to the naked eye.

Conclusion

We performed artificial aging of TiO_2 and linseed oil based systems to investigate the mechanisms of degradation under visible and UV light. We used FT-IR to identify characteristic markers of degradation: the formation of free fatty acids visible at 1710 cm^{-1}, an increase in the spectral region 1670–1610 cm^{-1} associated with ν(C=C) of conjugated dienes and changes in the triglyceride ester linkage region centered at 1168 cm^{-1}. Both anatase and rutile TiO_2 based samples showed these characteristic markers of degradation under the visible and UV–vis light conditions used in these experiments. By measuring the change in intensity of characteristic degradation FT-IR peaks, we showed that anatase and rutile based paints facilitate similar rates of linseed oil degradation. The surface alteration of the paint film was monitored by SEM, highlighting surfacing of pigment particles due to oil loss and confirming the activity of rutile based paints. Through computational calculations, we characterized a complex formed by attaching oleic acid to the surface of anatase TiO_2 in a bidentate configuration. The electronic structure of this complex allowed for visible light facilitated electron injection into the TiO_2 conduction band and the subsequent formation of an oleic acid cation radical which can undergo further degradative reaction with water and desorb from the surface. This excited electron can form ROS through proton assisted reaction with oxygen and facilitate the degradation of the oil binder. Through this combination of methods, we have developed a better understanding of the risk that both anatase and rutile TiO_2 containing paints face under low intensity illumination conditions.

Abbreviations

DFT: Density functional theory; ATR-FT-IR: Attenuated total reflection fourier transform infrared spectroscopy; SEM: Scanning electron microscopy; ROS: Radical oxygen species; GGA: Generalized gradient approximation; PBE: Perdew-Burke-Ernzerhof; Xc: Exchange correlation; G09: Gaussian 09; HOMO: The highest occupied molecular orbitals; LUMO: Lowest unoccupied molecular orbitals; DOS: Density of states; pDOS: Partial DOS.

Supplementary Information

The online version contains supplementary material available at https://doi.org/10.1186/s40494-022-00733-2.

Additional file 1: Figure S1. Setup of aging chamber. **Figure S2.** Spectra of vis lighting condition. **Figure S3.** Spectra of UV–vis lighting condition. **Figure S4.** Structure of **(a)** linseed oil and **(b)** its component fatty acids. **Figure S5.** DOS comparison between the calculation carried out at Γ point with 10A of vacuum, with 20A of vacuum and with a k-point grid of 2x2x1 and 10A of vacuum. **Figure S6.** Vis **(a)** and UV-vis **(b)** aging of BaSO4 based paints. **Figure S7.** Vis and UV–vis aged anatase **(a, b)** and rutile **(c, d)** paint films. **Figure S8.** Dark aged **(a)** anatase, **(b)** rutile, **(c)** BaSO4, and **(d)** linseed oil films. **Table S1.** Frontier energy levels and HOMO–LUMO gap for linseed oil component acids calculated with B3YLP functionals.

Acknowledgements
We thank the staff of the Peggy Guggenheim Collection (Venice, Italy), especially Luciano Pensabene, for their generous assistance and access to *Eyes in the Heat*, as well as other early 20th century works.

Author contributions
TS, conducted the experiments, sample characterization and computational modeling as well as wrote the manuscript. FR advised and assisted with conceptualization and experimental details, SEM and FT-IR interpretation, and wrote, reviewed and edited the manuscript. EM provided software assistance and computational methods advise. KS provided project administration and manuscript review. SF conceptualized and supervised computational aspects of the research, provided software assistance and wrote, reviewed and edited the manuscript. CM conceptualized the research approach and supervised experimental work. KG conceptualized research appraoch, supervised experimental work and interpretation and wrote, reviewed and edited the manuscript. All authors read and approved the final manuscript.

Funding
This work was supported by the National Science Foundation (NSF) Partnerships for International Research and Education (PIRE) program under Grant number 1743748. The FT-IR work was performed in the Keck II facility of the NUANCE center at Northwestern University**,** which has received support from the SHyNE Resource (NSF ECCS-2025633), the International Institute for Nanotechnology (IIN), and Northwestern's MRSEC program (NSF DMR-1720139). The SEM work was done at the LUNA laboratory of the University.

Availability of data and materials
The datasets used and/or analyzed during the current study are available from the corresponding author on reasonable request.

Declarations

Competing interests
All authors have read and approved this manuscript. The authors of this paper have no competing interests to declare.

Author details
[1]Department of Materials Science and Engineering, Northwestern University, Evanston, IL 60208, USA. [2]Istituto CNR di Scienze e Tecnologie Chimiche (CNR-SCITEC), via Elce di Sotto 8, 06123 Perugia, Italy. [3]Istituto CNR di Heritage Science (CNR-ISPC), Via Cardinale Guglielmo Sanfelice 8, 80134 Naples, Italy. [4]Department of Civil and Environmental Engineering, Northwestern University, 2145 Sheridan Road, Evanston, IL 60208, USA.

Received: 28 March 2022 Accepted: 5 June 2022
Published online: 29 June 2022

References

1. FitzHugh EW. Artists' pigments, vol. 3. Washington: National Gallery of Art; 2012.
2. Pelaez M, Nolan NT, Pillai SC, Seery MK, Falaras P, Kontos AG, Dunlop PSM, Hamilton JWJ, Byrne JA, O'Shea K, Entezari MH, Dionysiou DD. A review on the visible light active titanium dioxide photocatalysts for environmental applications. Appl Catal B Environ. 2012;125:331–49. https://doi.org/10.1016/j.apcatb.2012.05.036.
3. van Driel BA. Titanium dioxide friend or foe. Delft University of Technology. 2019.
4. Rosi F, Grazia C, Fontana R, Gabrieli F, Pensabene Buemi L, Pampaloni E, Romani A, Stringari C, Miliani C. Disclosing Jackson Pollock's palette in alchemy (1947)by non-invasive spectroscopies. Herit Sci. 2016. https://doi.org/10.1186/s40494-016-0089-y.
5. Martins A, Coddington J, Van der Snickt G, van Driel B, McGlinchey C, Dahlberg D, Janssens K, Dik J. Jackson Pollock's number 1A, 1948: a non-invasive study using macro-X-ray fluorescence mapping (MA-XRF) and multivariate curve resolution-alternating least squares (MCR-ALS) analysis. Herit Sci. 2016. https://doi.org/10.1186/s40494-016-0105-2.
6. Morsch S, van Driel BA, van den Berg KJ, Dik J. Investigating the photocatalytic degradation of oil paint using ATR-IR and AFM-IR. ACS Appl Mater Interfaces. 2017;9(11):10169–79. https://doi.org/10.1021/acsami.7b00638.
7. van Driel BA, Wezendonk TA, van den Berg KJ, Kooyman PJ, Gascon J, Dik J. Determination of early warning signs for photocatalytic degradation of titanium white oil paints by means of surface analysis. Spectrochim Acta A Mol Biomol Spectrosc. 2017;172:100–8. https://doi.org/10.1016/j.saa.2016.04.026.
8. van Driel BA, Kooyman PJ, van den Berg KJ, Schmidt-Ott A, Dik J. A quick assessment of the photocatalytic activity of TiO 2 pigments—from lab to conservation studio! Microchem J. 2016;126:162–71. https://doi.org/10.1016/j.microc.2015.11.048.
9. Etacheri V, Di Valentin C, Schneider J, Bahnemann D, Pillai SC. Visible-light activation of TiO2 photocatalysts: advances in theory and experiments. J Photochem Photobiol C Photochem Rev. 2015;25:1–29. https://doi.org/10.1016/j.jphotochemrev.2015.08.003.
10. Di Valentin C, Tilocca A, Selloni A, Beck TJ, Klust A, Batzill M, Losovyj Y, Diebold U. Adsorption of water on reconstructed rutile TiO_2 (011) − (2 × 1): TiO double bonds and surface reactivity. J Am Chem Soc. 2005;127(27):9895–903. https://doi.org/10.1021/ja0511624.
11. Nolan M, Deskins NA, Schwartzenberg KC, Gray KA. Local interfacial structure influences charge localization in titania composites: beyond the band alignment paradigm. J Phys Chem C. 2016;120(3):1808–15. https://doi.org/10.1021/acs.jpcc.5b12326.
12. Zhang X. Photocatalytical effect of TiO2 pigments on the surface of paint films. 2013.
13. Luttrell T, Halpegamage S, Tao J, Kramer A, Sutter E, Batzill M. Why is anatase a better photocatalyst than rutile?—model studies on epitaxial TiO2 films. Sci Rep. 2015. https://doi.org/10.1038/srep04043.
14. Modan EM. Review on the titanium oxide for catalytic applications. Univ Pitesti Sci Bull Automot Ser. 2019;29(1):1–10. https://doi.org/10.26825/bup.ar.2019.007.
15. Gong X-Q, Selloni A, Vittadini A. Density functional theory study of formic acid adsorption on anatase TiO_2 (001): geometries, energetics, and effects of coverage, hydration, and reconstruction. J Phys Chem B. 2006;110(6):2804–11. https://doi.org/10.1021/jp056572t.
16. Amat A, Miliani C, Romani A, Fantacci S. DFT/TDDFT investigation on the UV-Vis absorption and fluorescence properties of alizarin dye. Phys Chem Chem Phys. 2015;17(9):6374–82. https://doi.org/10.1039/C4CP04728A.
17. Gurdal Y, Iannuzzi M. DFT-based theoretical simulations for photocatalytic applications using TiO2. In: Janus M, editor. Titanium dioxide. Richardson: InTech; 2017.
18. Nilsing M, Lunell S, Persson P, Ojamäe L. Phosphonic acid adsorption at the TiO2 anatase (101) surface investigated by periodic hybrid HF-DFT computations. Surf Sci. 2005;582(1–3):49–60. https://doi.org/10.1016/j.susc.2005.02.044.
19. Yao M, Ji Y, Wang H, Ao Z, Li G, An T. Adsorption mechanisms of typical carbonyl-containing volatile organic compounds on anatase TiO_2 (001) surface: a DFT investigation. J Phys Chem C. 2017;121(25):13717–22. https://doi.org/10.1021/acs.jpcc.7b02964.
20. de Viguerie L, Payard PA, Portero E, Walter Ph, Cotte M. The drying of linseed oil investigated by fourier transform infrared spectroscopy: historical recipes and influence of lead compounds. Prog Org Coat. 2016;93:46–60. https://doi.org/10.1016/j.porgcoat.2015.12.010.
21. Giannozzi P, Baroni S, Bonini N, Calandra M, Car R, Cavazzoni C, Ceresoli D, Chiarotti GL, Cococcioni M, Dabo I, Corso AD, de Gironcoli S, Fabris S, Fratesi G, Gebauer R, Gerstmann U, Gougoussis C, Kokalj A, Lazzeri M, Martin-Samos L, Marzari N, Mauri F, Mazzarello R, Paolini S, Pasquarello A, Paulatto L, Sbraccia C, Scandolo S, Sclauzero G, Seitsonen AP, Smogunov A, Umari P, Wentzcovitch RM. QUANTUM ESPRESSO: a modular and open-source software project for quantum simulations of materials. J Phys Condens Matter. 2009;21(39):395502.
22. Perdew JP, Burke K, Ernzerhof M. Generalized gradient approximation made simple. Phys Rev Lett. 1996;77(18):3865–8. https://doi.org/10.1103/PhysRevLett.77.3865.
23. Vittadini A, Selloni A, Rotzinger FP, Grätzel M. Structure and energetics of water adsorbed at TiO 2 anatase 101 and 001 surfaces. Phys Rev Lett. 1998;81(14):2954–7. https://doi.org/10.1103/PhysRevLett.81.2954.

24. Dal Corso A. Pseudopotentials periodic table: from H to Pu. Comput Mater Sci. 2014;95:337–50. https://doi.org/10.1016/j.commatsci.2014.07.043.
25. Frisch MJ, Trucks GW, Schlegel HB, Scuseria GE, Robb MA, Cheeseman JR, Scalmani G, Barone V, Petersson GA, Nakatsuji H, Li X, Caricato M, Marenich AV, Bloino J, Janesko BG, Gomperts R, Mennucci B, Hratchian HP, Ortiz JV, Izmaylov AF, Sonnenberg JL, Williams, Ding F, Lipparini F, Egidi F, Goings J, Peng B, Petrone A, Henderson T, Ranasinghe D, Zakrzewski VG, Gao J, Rega N, Zheng G, Liang W, Hada M, Ehara M, Toyota K, Fukuda R, Hasegawa J, Ishida M, Nakajima T, Honda Y, Kitao O, Nakai H, Vreven T, Throssell K, Montgomery Jr JA, Peralta JE, Ogliaro F, Bearpark MJ, Heyd JJ, Brothers EN, Kudin KN, Staroverov VN, Keith TA, Kobayashi R, Normand J, Raghavachari K, Rendell AP, Burant JC, Iyengar SS, Tomasi J, Cossi M, Millam JM, Klene M, Adamo C, Cammi R, Ochterski JW, Martin RL, Morokuma K, Farkas O, Foresman JB, Fox DJ. Gaussian 16 Rev. B.01. Wallingford, CT. 2016.
26. Becke AD. Density-functional thermochemistry. III. the role of exact exchange. J Chem Phys. 1993;98(7):5648–52. https://doi.org/10.1063/1.464913.
27. Vosko SH, Wilk L, Nusair M. Accurate spin-dependent electron liquid correlation energies for local spin density calculations: a critical analysis. Can J Phys. 1980;58(8):1200–11. https://doi.org/10.1139/p80-159.
28. Lee C, Yang W, Parr RG. Development of the Colle-Salvetti correlation-energy formula into a functional of the electron density. Phys Rev B. 1988;37(2):785–9. https://doi.org/10.1103/PhysRevB.37.785.
29. Stephens PJ, Devlin FJ, Chabalowski CF, Frisch MJ. Ab initio calculation of vibrational absorption and circular dichroism spectra using density functional force fields. J Phys Chem. 1994;98(45):11623–7. https://doi.org/10.1021/j100096a001.
30. Petersson GA, Al-Laham MA. A complete basis set model chemistry. II. Open-shell systems and the total energies of the first-row atoms. J Chem Phys. 1991;94(9):6081–90. https://doi.org/10.1063/1.460447.
31. Hanwell MD, Curtis DE, Lonie DC, Vandermeersch T, Zurek E, Hutchison GR. Avogadro: an advanced semantic chemical editor, visualization, and analysis platform. J Cheminformatics. 2012;4(1):17. https://doi.org/10.1186/1758-2946-4-17.
32. Meilunas RJ, Bentsen JG, Steinberg A. Analysis of aged paint binders by FTIR spectroscopy. Stud Conserv. 1990;35(1):33–51. https://doi.org/10.1179/sic.1990.35.1.33.
33. Mazzeo R, Prati S, Quaranta M, Joseph E, Kendix E, Galeotti M. Attenuated total reflection micro FTIR characterisation of pigment-binder interaction in reconstructed paint films. Anal Bioanal Chem. 2008;392(1–2):65–76. https://doi.org/10.1007/s00216-008-2126-5.
34. van den Berg JDJ, van den Berg KJ, Boon JJ. Determination of the degree of hydrolysis of oil paint samples using a two-step derivatisation method and on-column GC/MS. Prog Org Coat. 2001;41(1–3):143–55. https://doi.org/10.1016/S0300-9440(01)00140-0.
35. van Dam EP, van den Berg KJ, Proaño Gaibor AN, van Bommel M. Analysis of triglyceride degradation products in drying oils and oil paints using LC–ESI-MS. Int J Mass Spectrom. 2017;413:33–42. https://doi.org/10.1016/j.ijms.2016.09.004.
36. Fjällström P, Andersson B, Nilsson C, Andersson K. Drying of linseed oil paints: a laboratory study of aldehyde emissions. Ind Crops Prod. 2002;16(3):173–84. https://doi.org/10.1016/S0926-6690(02)00035-3.
37. Zumbühl S, Scherrer NC, Eggenberger U. Derivatization technique to increase the spectral selectivity of two-dimensional fourier transform infrared focal plane array imaging: analysis of binder composition in aged oil and tempera paint. Appl Spectrosc. 2014;68(4):458–65. https://doi.org/10.1366/13-07280.
38. Bonaduce I, Carlyle L, Colombini MP, Duce C, Ferrari C, Ribechini E, Selleri P, Tiné MR. New insights into the ageing of linseed oil paint binder: a qualitative and quantitative analytical study. PLoS ONE. 2012;7(11): e49333. https://doi.org/10.1371/journal.pone.0049333.
39. Daoud S, Bou-maroun E, Dujourdy L, Waschatko G, Billecke N, Cayot P. Fast and direct analysis of oxidation levels of oil-in-water emulsions using ATR-FTIR. Food Chem. 2019;293:307–14. https://doi.org/10.1016/j.foodchem.2019.05.005.
40. Lin-Vien D, Colthup NB, Fateley WG, Grasselli JG. The handbook of infrared and raman characteristic frequencies of organic molecules. Amsterdam: Elsevier; 1991.
41. Berto BM, Garcia RKA, Fernandes GD, Barrera-Arellano D, Pereira GG. Linseed oil: characterization and study of its oxidative degradation. Grasas Aceites. 2020;71(1):337. https://doi.org/10.3989/gya.1059182.
42. Hayati IN, Man YBC, Tan CP, Aini IN. Monitoring peroxide value in oxidized emulsions by Fourier transform infrared spectroscopy. Eur J Lipid Sci Technol. 2005;107(12):886–95. https://doi.org/10.1002/ejlt.200500241.
43. Ioakimoglou E, Boyatzis S, Argitis P, Fostiridou A, Papapanagiotou K, Yannovits N. Thin-film study on the oxidation of linseed oil in the presence of selected copper pigments. Chem Mater. 1999;11(8):2013–22. https://doi.org/10.1021/cm9806578.
44. Morales-García Á, Valero R, Illas F. An empirical, yet practical way to predict the band gap in solids by using density functional band structure calculations. J Phys Chem C. 2017;121(34):18862–6. https://doi.org/10.1021/acs.jpcc.7b07421.
45. Orlova Y, Harmon RE, Broadbelt LJ, Iedema PD. Review of the kinetics and simulations of linseed oil autoxidation. Prog Org Coat. 2021;151: 106041. https://doi.org/10.1016/j.porgcoat.2020.106041.
46. Juita, Dlugogorski BZ, Kennedy EM, Mackie JC. Low temperature oxidation of linseed oil: a review. Fire Sci Rev. 2012;1(1):3. https://doi.org/10.1186/2193-0414-1-3.
47. Baij L, Chassouant L, Hermans JJ, Keune K, Iedema PD. The concentration and origins of carboxylic acid groups in oil paint. RSC Adv. 2019;9(61):35559–64. https://doi.org/10.1039/C9RA06776K.
48. McGill PR, Idriss H. DFT study of carboxylic acids modes of adsorption on rutile TiO2(011) surfaces. Surf Sci. 2008;602(24):3688–95. https://doi.org/10.1016/j.susc.2008.10.010.
49. Ignatchenko AV. Density functional theory study of carboxylic acids adsorption and enolization on monoclinic zirconia surfaces. J Phys Chem C. 2011;115(32):16012–8. https://doi.org/10.1021/jp203381h.
50. Boyatzis S, Ioakimoglou E, Argitis P. UV exposure and temperature effects on curing mechanisms in thin linseed oil films: spectroscopic and chromatographic studies. J Appl Polym Sci. 2002;84(5):936–49. https://doi.org/10.1002/app.10117.
51. Dupuis A, Perrin F-X, Ulloa Torres A, Habas J-P, Belec L, Chailan J-F. Photo-oxidative degradation behavior of linseed oil based epoxy resin. Polym Degrad Stab. 2017;135:73–84. https://doi.org/10.1016/j.polymdegradstab.2016.11.021.
52. van Driel BA, van den Berg KJ, Smout M, Dekker N, Kooyman PJ, Dik J. Investigating the effect of artists' paint formulation on degradation rates of TiO2-based oil paints. Herit Sci. 2018;6(1):21. https://doi.org/10.1186/s40494-018-0185-2.
53. Almquist CB, Biswas P. Role of synthesis method and particle size of nanostructured TiO2 on its photoactivity. J Catal. 2002;212(2):145–56. https://doi.org/10.1006/jcat.2002.3783.
54. Carp O. Photoinduced reactivity of titanium dioxide. Prog Solid State Chem. 2004;32(1–2):33–177. https://doi.org/10.1016/j.progsolidstchem.2004.08.001.
55. Lauridsen CB, Sanyova J, Simonsen KP. Analytical study of modern paint layers on metal knight shields: the use and effect of titanium white. Spectrochim Acta A Mol Biomol Spectrosc. 2014;124:638–45. https://doi.org/10.1016/j.saa.2014.01.077.
56. Pappas SP, Winslow FH. Photodegradation and photostabilization of coatings, vol. 151. Washington, DC: American Chemical Society; 1981. https://doi.org/10.1021/bk-1981-0151.
57. Zhang Z, Yates JT. Band bending in semiconductors: chemical and physical consequences at surfaces and interfaces. Chem Rev. 2012;112(10):5520–51. https://doi.org/10.1021/cr3000626.
58. Dlugogorski BZ, Kennedy EM, Mackie JC. Low temperature oxidation of linseed oil: a review. Fire Sci. 2012. https://doi.org/10.1186/2193-0414-1-3.
59. Bacci M, Picollo M, Trumpy G, Tsukada M, Kunzelman D. Non-invasive identification of white pigments on 20th-century oil paintings by using fiber optic reflectance spectroscopy. J Am Inst Conserv. 2007;46(1):27–37. https://doi.org/10.1179/019713607806112413.
60. Buchholz M, Xu M, Noei H, Weidler P, Nefedov A, Fink K, Wang Y, Wöll C. Interaction of carboxylic acids with rutile TiO2(110): IR-investigations of terephthalic and benzoic acid adsorbed on a single crystal substrate. Surf Sci. 2016;643:117–23. https://doi.org/10.1016/j.susc.2015.08.006.
61. Haque SA, Tachibana Y, Willis RL, Moser JE, Grätzel M, Klug DR, Durrant JR. Parameters influencing charge recombination kinetics in dye-sensitized nanocrystalline titanium dioxide films. J Phys Chem B. 2000;104(3):538–47. https://doi.org/10.1021/jp991085x.

62. Christopher P, Xin H, Marimuthu A, Linic S. Singular characteristics and unique chemical bond activation mechanisms of photocatalytic reactions on plasmonic nanostructures. Nat Mater. 2012;11(12):1044–50. https://doi.org/10.1038/nmat3454.
63. Jacobsen AE. Titanium dioxide pigments: correlation between photochemical reactivity and chalking. Ind Eng Chem. 1949;41(3):523–6. https://doi.org/10.1021/ie50471a018.
64. Voltz HG, Kaempf G, Fitzky HG, Klaeren A. The chemical nature of chalking in the presence of titanium dioxide pigments. Photodegrad Photostab Coat. 1981;151(Chapter 12):163–82.

Publisher's Note